RESEARCH ARTICLE SUMMARY

PLANT SCIENCE

Enhancing rice panicle branching and grain yield through tissue-specific brassinosteroid inhibition

Xiaoxing Zhang†, Wenjing Meng†, Dapu Liu†, Dezhuo Pan†, Yanzhao Yang, Zhuo Chen, Xiaoding Ma, Wenchao Yin, Mei Niu, Nana Dong, Jihong Liu, Weifeng Shen, Yuqin Liu, Zefu Lu, Chengcai Chu, Qian Qian*, Mingfu Zhao*, Hongning Tong*

INTRODUCTION: Crop breeding is essentially the art of balancing various traits to achieve the best performance in plants. However, achieving the optimal balance is challenging owing to complex relationships among traits. One major hurdle is the trade-offs among various traits such as between grain size and grain number. Brassinosteroids (BRs), a class of steroid hormones, promote grain size and have been demonstrated to enhance crop yield. Despite their potential, the pleiotropic effects of BRs have hindered their use in crop improvement, and their role in regulating grain number remains unclear.

RATIONALE: Clustered-spikelet rice (CL) is a distinctive germplasm with historical importance, producing multiple grains from a single position without affecting grain size. The causal gene for CL has remained elusive for almost a century. We hypothesized that dissecting the molecular genetics of CL could provide insights into panicle branching and potentially unlock the trade-off between grain size and number. Observations of weakly clustered growth in BR-deficient plants suggested a possible role of BRs in controlling this trait. Understanding the mechanism behind CL occurrence could offer new insights into BR function and its role in controlling similar growth patterns in various species. Cloning the *CL* gene is a crucial first step in exploring these possibilities.

RESULTS: We successfully cloned the causal gene for CL through extensive screening of CL suppressor mutants. Genomic analysis revealed that CL is associated with complex structural variations in chromosomes, activating the BR catabolic gene *BRASSINOSTEROID-DEFICIENT DWARF3* (*BRD3*) in secondary branch meristems. Spatial-specific activation of *BRD3* promotes grain number without the common negative effects of BR deficiency on grain size. We uncovered a tissue-specific BR pathway that supports this function, involving the BR signaling inhibitor kinase GSK3/SHAGGY-LIKE KINASE2 (GSK2), which phosphorylates and stabilizes the OsMADS1 transcriptional factor. OsMADS1, in turn, targets and promotes the *TERMINAL FLOWER1*-like gene *RICE CENTRORADIALIS2* (*RCN2*) to suppress meristem identity. Introduction of CL into different backgrounds substantially improved rice yield. Additionally, we found consistent alterations in BR content in pepper and rose with clustered growth patterns, suggesting a broader role of BRs in controlling this phenotype in nature.

CONCLUSION: The identification of complex structural variations preceding *BRD3* explains previous unsuccessful attempts to clone the gene. Our research unveils a groundbreaking role of BRs in coordinating panicle branching and grain number through precise meristem transitions. We describe a tissue-specific BR pathway (*BRD3*-BR-GSK2-OsMADS1-*RCN2*) that underpins this previously unknown function. The positive and negative roles of BRs in regulating grain size and number, respectively, represent a crucial trade-off mechanism. Notably, this spatially targeted mechanism within the BR pathway enhances grain number without compromising size. Therefore, manipulating BR distribution provides effective breeding strategies for finely tuning crop traits, ultimately boosting crop yield. Our findings showcase the efficacy of tissue-specific hormonal manipulation in overcoming trade-offs among various traits and unlocking crop yield potential. Changes in BR levels may represent a fundamental mechanism governing natural inflorescence architecture. ■

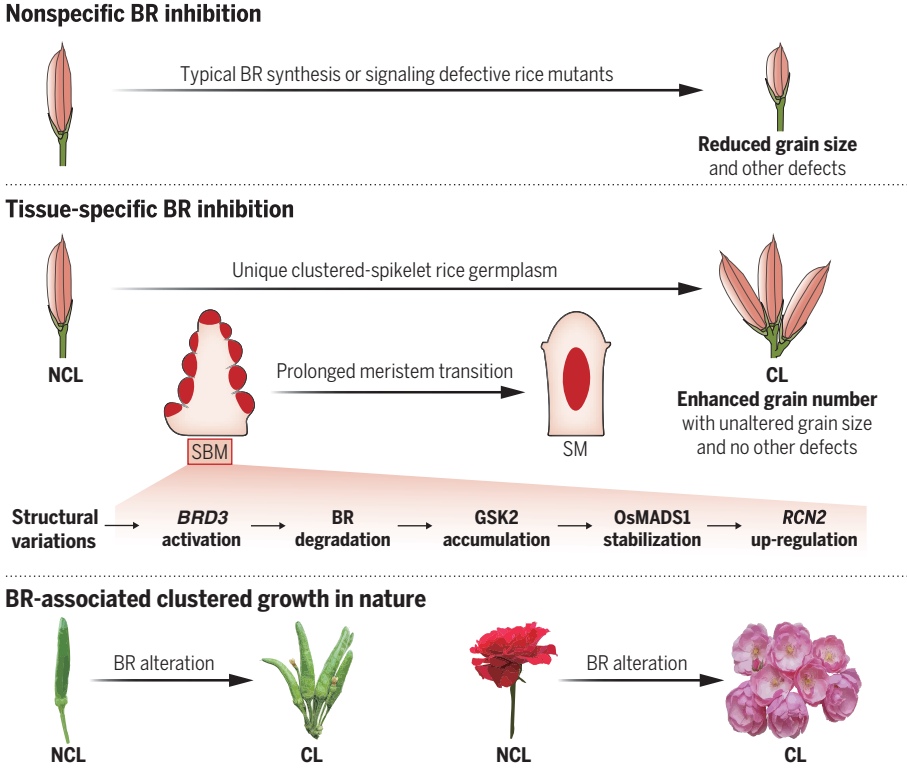

Tissue-specific BR inhibition promotes rice panicle branching. Structural variations in CL activate *BRD3* in specific tissues (red) such as secondary branch meristems (SBMs), where it causes BR degradation, GSK2 accumulation, OsMADS1 stabilization, and *RCN2* up-regulation. This affects spikelet meristem (SM) identity, prolonging the SBM to SM transition, increasing panicle branching and grain number without affecting grain size. BR change may be associated with the clustered growth in various plants.

The list of author affiliations is available in the full article online.
*Corresponding author. Email: tonghongning@caas.cn (H.T.); zhmingfu@163.com (M.Z.); qianqian@caas.cn (Q.Q.)
†These authors contributed equally to this work.
Cite this article as X. Zhang *et al.*, *Science* **383**, eadk8838 (2024). DOI: 10.1126/science.adk8838

READ THE FULL ARTICLE AT
https://doi.org/10.1126/science.adk8838

RESEARCH ARTICLE

PLANT SCIENCE

Enhancing rice panicle branching and grain yield through tissue-specific brassinosteroid inhibition

Xiaoxing Zhang[1]†, Wenjing Meng[1]†, Dapu Liu[1]†, Dezhuo Pan[2]†, Yanzhao Yang[1], Zhuo Chen[3], Xiaoding Ma[1], Wenchao Yin[1], Mei Niu[1], Nana Dong[1], Jihong Liu[1], Weifeng Shen[2], Yuqin Liu[2], Zefu Lu[1], Chengcai Chu[3], Qian Qian[1]*, Mingfu Zhao[2]*, Hongning Tong[1]*

Crop yield potential is constrained by the inherent trade-offs among traits such as between grain size and number. Brassinosteroids (BRs) promote grain size, yet their role in regulating grain number is unclear. By deciphering the clustered-spikelet rice germplasm, we show that activation of the BR catabolic gene *BRASSINOSTEROID-DEFICIENT DWARF3* (*BRD3*) markedly increases grain number. We establish a molecular pathway in which the BR signaling inhibitor GSK3/SHAGGY-LIKE KINASE2 phosphorylates and stabilizes OsMADS1 transcriptional factor, which targets *TERMINAL FLOWER1*-like gene *RICE CENTRORADIALIS2*. The tissue-specific activation of *BRD3* in the secondary branch meristems enhances panicle branching, minimizing negative effects on grain size, and improves grain yield. Our study showcases the power of tissue-specific hormonal manipulation in dismantling the trade-offs among various traits and thus unleashing crop yield potential in rice.

Rice (*Oryza sativa*) is an essential staple crop, feeding more than half of the world's population (*1*). With global population growth and diminishing arable land, it is crucial to enhance rice grain yield per unit area to ensure global food security. During the development of the rice panicle, the inflorescence meristem produces multiple primary and secondary branches. Panicle branching determines grain number, one of the determinants of grain yield. Therefore, one promising approach to increase grain yield is by enhancing panicle branching. The identification of genes controlling panicle branching, such as *Grain number1a* (*Gn1a*) and *DENSE PANICLE 1* (*DEP1*), has exemplified the success of this approach (*2*, *3*). However, after extensive breeding efforts using these genes, rice yield has reached a plateau, primarily attributed to the intricate trade-offs among various traits that prove resistant to conventional breeding interventions. Tackling this formidable challenge requires an exploration of pioneering genetic reservoirs sourced from a wide array of germplasm resources to facilitate subsequent advancements.

Brassinosteroids (BRs) are a class of steroid phytohormones that play diverse roles in plant growth and development (*4*–*6*). BR responses require BR signaling, in which GSK3/SHAGGY-like kinases, such as BRASSINOSTEROID INSENSITIV2 in the model plant *Arabidopsis* (*Arabidopsis thaliana*) and GSK3/SHAGGY-LIKE KINASE2 (GSK2) in rice, act as the central inhibitors (*7*, *8*) targeting different substrates to modulate various BR responses (*5*, *9*). In cereal crops such as rice, BRs regulate important agronomic traits such as plant height, leaf angle, and grain size (*5*). Rice mutants with defective BR synthesis or signaling usually show dwarfism, upright leaves, and small grains (*10*–*12*). Despite the promising results achieved in major crops such as rice, maize (*Zea mays*), and wheat (*Triticum aestivum*) using BR-related gene resources for yield improvement (*13*–*15*), the small-grain phenotypes limit the utility of BR mutants for enhancing grain yield. In addition, it remains largely unclear how BRs regulate panicle branching and grain number. Together with additional potential influences such as stress tolerance, the pleiotropic effects of BRs present great challenges for the effective utilization of BR regulatory genes (*5*).

Unlike the common single-grained rice, clustered-spikelet rice (CL), also known as compound-spikelet rice, wheat-spike rice, or SAN-LI-QI (meaning triple-grain-miracle in Chinese), is an unusual rice germplasm possessing an extraordinary trait of multiple (often triple) complete spikelets or grains clustered on the panicles. Since its description early in 1931, the distinctive character of CL has been used to construct a genetic linkage map by worldwide rice geneticists (*16*–*19*). Owing to its potential for improving grain productivity, researchers have made numerous efforts to identify and clone the gene (*CL*) responsible for this trait. Although several studies have successfully mapped the *CL* locus to a specific region on chromosome 6 (*20*–*24*), the gene itself has eluded cloning attempts, for reasons that are unclear.

Here, we report our successful cloning of the causal gene for CL by large-scale screening of CL suppressor mutants. We show that CL is associated with complex chromosome structural variations, which activate the expression of the BR catabolic gene *BRASSINOSTEROID-DEFICIENT DWARF3* (*BRD3*) in the secondary branch meristems and pedicels. Notably, the spatial-specific activation of *BRD3* promotes grain number while avoiding the commonly seen negative effects of BR deficiency on grain size and grain quality. Moreover, we establish a complete BR pathway for mediating BR regulation of panicle branching. Furthermore, we demonstrate that introduction of *CL* into various backgrounds, either containing *Gn1a* gene or not, can substantially improve rice yield.

Results

CL confers enhanced panicle branching and grain yield

CL1 represents a typical CL variety characterized by clustered growth, primarily consisting of three grains. To facilitate comparisons, we generated a non-CL variety (NCL1) by using CL1 as the recurrent parent. Apart from the distinct panicle morphology, no other notable differences were observed between NCL1 and CL1 (Fig. 1, A and B). The clustered growth in CL1 predominantly occurred at the terminus of the secondary branch, where a pair of closely fused spikelets formed, with a third spikelet attached nearby (Fig. 1, C and D). Additionally, the tertiary branch was frequently observed in CL1 but not in NCL1 plants (Fig. 1E). Moreover, pedicels attached to the spikelets in CL1 were shorter than those of NCL1 (Fig. 1F).

CL1 showed a 28.2% increase in grain number per panicle compared to NCL1 (Fig. 1G), which was attributed to a greater number of secondary panicle branches (35.2% increase) and associated spikelets, but not the primary branches (Fig. 1, H to J). No significant differences were detected between NCL1 and CL1 for other traits such as panicle length, panicle number, heading date, and 1000-grain weight (Fig. 1, K to M, and fig. S1). The specific enhancement of grain number in CL1 resulted in a 20.1% increase in grain yield per plant in Beijing (north of China, 2021), 21.7% increase in Sanya (south of China, 2022), and 12.8% increase in Fuzhou (south of China, 2020) compared to NCL1 (Fig. 1, N and O, and fig. S1). These findings were further confirmed in the field plot tests. Under the field conditions, except for the CL phenotype, no other differences were observed throughout NCL1 and CL1 growth (Fig. 1P). Compared to NCL1, CL1 grain yield per hectare averaged 20.96, 17.99, and 11.27% higher in Beijing, Sanya, and Fuzhou, respectively (Fig. 1Q and fig. S1). Regarding grain quality, no significant differences were detected between NCL1 and CL1 in terms of grain chalkiness, amylose content, gel consistency,

[1]State Key Laboratory of Crop Gene Resources and Breeding, Institute of Crop Sciences, Chinese Academy of Agricultural Sciences, Beijing 100081, China. [2]Rice Research Institute, Fujian Academy of Agricultural Sciences, Fuzhou 350018, China. [3]Institute of Genetics and Developmental Biology, Chinese Academy of Sciences, Beijing 100101, China.
*Corresponding author. Email: tonghongning@caas.cn (H.T.); zhmingfu@163.com (M.Z.); qianqian@caas.cn (Q.Q.)
†These authors contributed equally to this work.

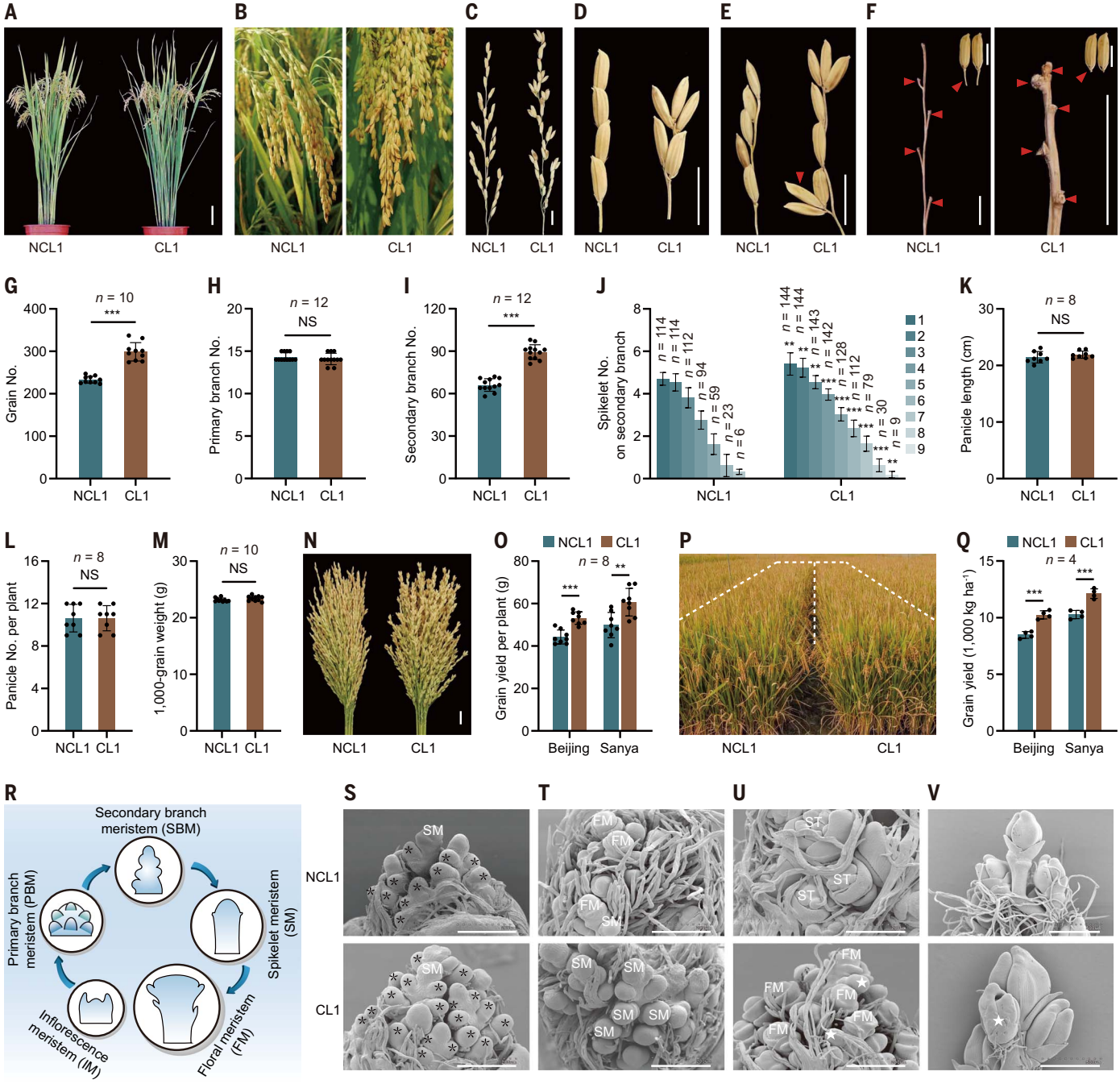

Fig. 1. CL promotes grain number and yield. (**A** to **Q**) Comparison of NCL1 and CL1 in terms of plant morphology (A), panicle (B), primary panicle branch (C), secondary panicle branch (D and E, arrowhead indicates a tertiary branch), pedicels (arrowheads in F), grain number per panicle (G), primary branch number per panicle (H), secondary branch number per panicle (I), spikelet number on each secondary branch (J), panicle length (K), panicle number (L), grain weight (M), a collection of 10 panicles (N), grain yield per plant (O), field performance (P), and grain yield per hectare (Q). For statistical data, error bars indicate standard deviation (SD). $^{**}P < 0.01$ and $^{***}P < 0.001$ by two-tailed *t* test. NS, not significant. Scale bars: 10 cm (A), 1 cm (C to E), 5 mm (F), and 2 cm (N). In J, the numbers (1 to 9) indicate the position of the secondary branch on the primary branch, with 1 representing the basal secondary branch. (**R**) A schematic diagram depicting the meristem development. (**S** to **V**) Scanning electron micrographs of panicle development process. *, SBM; ☆, additional SM; ST, stamen primordia. Scale bars: 200 μm (S to U) and 500 μm (V).

and gelatinization temperature, and only total protein content was slightly greater in CL1 (fig. S2). These results suggested that the CL trait has great potential for crop improvement, prompting us to explore the underlying mechanisms.

Prolonged branching time leads to increased grain number

During rice panicle development, a series of lateral meristems with distinct identities are sequentially generated (Fig. 1R). Inflorescence meristems first produce lateral primary branch meristems (PBMs). Subsequently, the newly initiated meristem from the PBM either acquires the identity of secondary branch meristem (SBM) or terminates as a spikelet meristem (SM). The SBM continues to generate next-order lateral meristems that will eventually

acquire the SM identity. Finally, the SM is transformed into a floral meristem (FM) (*25*–*27*). Scanning electron microscopic (SEM) observation identified excrescent SBMs in CL1 at the early stage of panicle development (fig. 1S). In addition, the transition from BM to SM was delayed in CL1 (Fig. 1, S to U). FMs were formed in NCL1 when the young panicle of CL1 was at the SM stage (Fig. 1T), and the FMs were already fully developed in NCL1 when the FMs in the young panicle of CL1 were formed (Fig. 1U). The delay in the transition from BM to SM resulted in prolonged time for generating more SBMs and even the formation of tertiary branches in CL1 (Fig. 1E). Furthermore, an additional SM developed adjacent to the terminal spikelet (Fig. 1U). Pedicel elongation was clear in NCL1 but barely observed in CL1 (Fig. 1V). On the basis of these observations, we concluded that three developmental phenomena drive CL formation: (i) the development of more SBMs, (ii) the initiation of supernumerary SM, and (iii) shortened pedicels.

Cloning the causal gene through screening CL suppressors

To help us track down the genetic basis for CL, we requested three other CL germplasms (CL2, CL3, CL4) from different sources, including one (CL3, IRIS_313-11403) from the 3000 Rice Genomes Project (3K-RG) (*28*). All three showed the typical CL phenotype, but they exhibited highly variable plant architecture and panicle morphology (fig. S3). We crossed them with each other and found that all F_1 plants derived from the different crosses retained the CL phenotype (fig. S3). By contrast, F_1 plants derived from crosses between CL1 and 9311, an NCL *indica* variety, or between CL1 and Zhonghua11 (ZH11), an NCL *japonica* variety, showed only a weak CL phenotype (WCL), characterized by clustered growth of two grains at the terminus of the panicle branches (figs. S4 and S5). In addition, in the crossed CL1 × ZH11 F_2 population, the segregation ratios (NCL:WCL:CL) were 65:131:45 (fig. S5), close to 1:2:1 (χ^2 = 0.0951664 < 5.99 at P = 0.05). These results suggested that the distinctive phenotype of these CL plants is determined by the same semidominant locus. However, our intense efforts using either map-based cloning or bulked-segregant analysis (BSA) by generating large populations or different crosses could only locate the locus to the ~22.85- to 23.85-Mb (megabase) region on chromosome 6 (fig. S6), like previously reported attempts (*21*–*24*). One possibility is that there exist complex chromosome structural variations around the region.

The failure of these routine cloning methods prompted us to design a strategic cloning roadmap by generating large-scale mutagenesis of CL1 for identifying the causal gene (Fig. 2A). From a population of 10,000 independent mutant lines (M_1) using sodium azide as the mutagen, examination of the phenotypes of the M_2 plants (16 for each line) led to the identification of two mutant lines that reverted to a wild-type NCL phenotype, which we designated *cl1-1* and *cl1-2* (Fig. 2B and fig. S7). By comparing the NCL and CL plants pooled from the F_2 population of the *cl1* × CL1 backcrosses, we found that, similar to NCL1, both *cl1-1* and *cl1-2* had significantly decreased grain number compared to CL1, owing to their smaller numbers of secondary branches (Fig. 2, D to F). Both mutants also showed identical plant architecture, panicle number, panicle length, and 1000-grain weight to those of NCL1 and CL1 (figs. S8 and S9 and Fig. 2G). In addition, the grain yield per plant of the two *cl1* mutants decreased by 16.4% to 27.7% compared to CL1 in Sanya (Fig. 2H). Because CL is controlled by a single semidominant gene, it is highly possible that the two mutants are revertants containing loss-of-function *CL* alleles. Indeed, F_2 populations derived from backcrosses with each mutant line showed segregation ratios (NCL:WCL:CL) close to 1:2:1 (Fig. 2C and fig. S10), indicating that both *cl1-1* and *cl1-2* carry recessive mutations at the *CL* locus.

To identify the mutations, we performed BSA by pooling NCL and CL plants with high-confidence phenotypes from the F_2 populations derived from *cl1-1* × CL1 and *cl1-2* × CL1 crosses, respectively. In the backcross populations, the *cl1-1* and *cl1-2* revertants were in the CL1 background, which could avoid the interference of other potentially related genes from the distant parents, such as had possibly occurred in map-based cloning. In addition, the chemical mutagen mostly caused single-nucleotide polymorphisms (SNPs), which would exclude the effect of potentially large variations on BSA results, such as had possibly occurred in the previous BSAs. Indeed, a limited number of associated SNPs or genes were identified in both analyses (Fig. 2A). Among them, we isolated one candidate gene (*LOC_Os06 g39880*), which was identified from both analyses and located in the previously determined region on chromosome 6 (Fig. 2, I and J). Notably, this gene was also the only candidate identified from all four BSAs (Fig. 2K). The associated SNPs identified from the BSAs resided in the candidate gene coding sequence and caused amino acid changes in both mutants (Fig. 2L). Therefore, this candidate gene *LOC_Os06 g39880*, previously reported as *BRD3* (*29*), was likely the CL-causal gene.

To verify this result, we used CRISPR-Cas9 technology to edit the *BRD3* gene in the CL1 background. All the edited lines (*cl-cc*) containing frameshift mutations displayed the NCL phenotype (Fig. 2M and fig. S11). Additionally, similar to NCL1, the *cl-cc* knockout mutants showed reduced grain number and yield per plant compared to CL1, whereas no significant differences were observed in terms of panicle length, panicle number, and grain weight (fig. S11). These analyses provide strong evidence that the identified candidate gene is responsible for both the CL phenotype and the enhanced grain productivity.

Up-regulated BRD3 *associated with structural variations in CL*

BRD3 encodes a functional BR-degrading enzyme, cytochrome P450 monooxygenase (CYP) 734A4 (*30*). Expression analysis using various tissues revealed that *BRD3* was highly expressed in reproductive tissues (fig. S12). In addition, treatment with brassinolide (BL), one of the active BRs, greatly induced *BRD3* expression, suggesting that *BRD3* is likely involved in the feedback regulation of BR homeostasis (fig. S13). Notably, *BRD3* expression was ~3- to 5-fold higher in the panicle of CL1 to CL4 compared with that of NCL1 and ZH11 (Fig. 3A). Consistent with the change in *BRD3* expression, the content of castasterone, one abundant BR form, was significantly lower in CL1 than in NCL1 (Fig. 3B). These analyses suggested that up-regulation of *BRD3* in CLs promotes BR degradation, resulting in the characteristic CL phenotypes.

To identify the underlying causal mutations responsible for CL traits, we conducted full-length sequencing of the *BRD3* gene in CL1 to CL4, as well as in several NCLs such as ZH11 and 9311. Numerous polymorphisms were detected in the promoter and coding regions; however, none of them was specific to the CLs (fig. S14). To gain a more comprehensive understanding, we used a combination of second- and third-generation sequencing techniques to reassemble the genome of this region. This approach revealed the presence of large structural variations in CL1, including a ~276-kb inversion, a deletion of ~12 kb, and an insertion of ~1.8 kb, located roughly 5 kb upstream of the *BRD3* promoter (Fig. 2L). Polymerase chain reaction (PCR) analysis confirmed that the inversion and deletion were present in all CLs but absent in any of the NCLs (fig. S15). CL3 was the sole CL accession identified from a combined population containing 3K-RG and a minicore rice collection (*31*), and was also the only one containing the deletion (fig. S16). This feature strongly suggests that the structural variations are responsible for activating *BRD3* expression in CLs. Thus, we will refer to the entire CL-associated locus as *CL* and use *BRD3* specifically for the gene in question.

Specifically activated BRD3 *in CL1's SBMs and pedicels*

BR-defective plants usually exhibit decreased grain size and plant height. Consistent with these phenotypes, previous studies have shown that *BRD3* overexpression in a constitutive manner strongly suppresses plant growth and development (*29*). However, we found

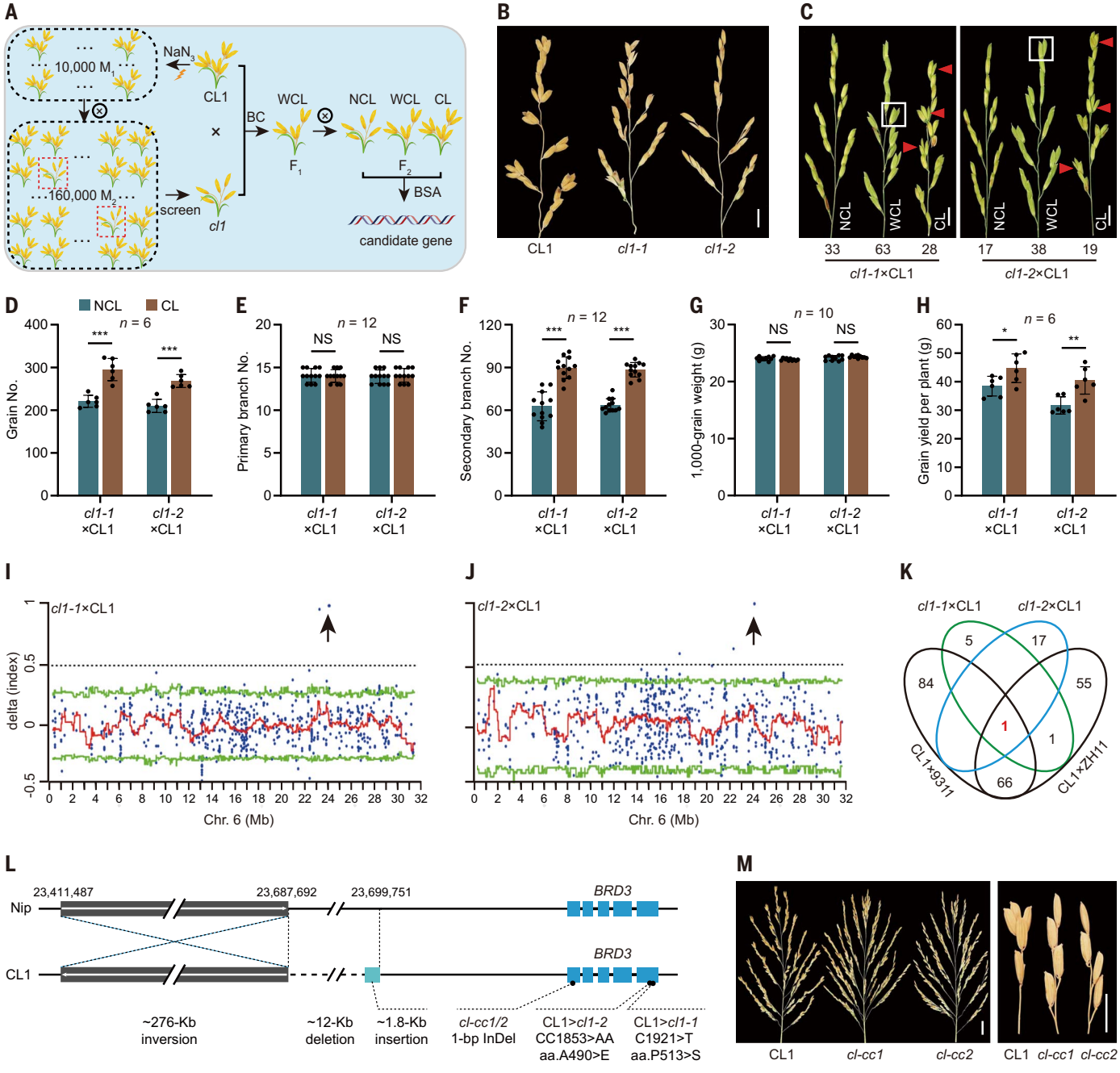

Fig. 2. Cloning of *BRD3* as the CL-causal gene. (**A**) Flow chart summarizing the cloning process. (**B**) Primary panicle branches of CL1 and the *cl1* mutants. Scale bars: 1 cm. (**C**) Phenotypic segregation and the individual numbers of each phenotype in the F_2 population. Scale bars: 1 cm. (**D** to **H**) Statistical data of grain number per panicle (D), primary branch number (E), secondary branch number (F), grain weight (G), and grain yield per plant (H) in two *cl1* mutants and CL1. *P < 0.05, **P < 0.01, and ***P < 0.001 by two-tailed t test. NS, not significant. NCL and CL plants were pooled from the F_2 population of the *cl1* × CL1 backcrosses. (**I** and **J**) Index maps on chromosome 6 generated in bulk segregant analyses (BSAs). Arrows indicate the same locus identified in two analyses. (**K**) Overlap in the candidate genes obtained from different BSAs. (**L**) Schematic diagram showing the structural variations 5 kb upstream of the *BRD3* gene in CL1. Mutations identified in different genotypes are presented. aa, amino acid. (**M**) Panicle morphology of *cl-cc* mutant lines, with secondary branches shown on right. Scale bars: 2 cm (left) and 1 cm (right).

no detectable differences in grain size and plant height among CL1, *cl1-1*, *cl1-2*, and NCL1 (Fig. 3, C to E, and fig. S17). Because CL is closely associated with shortened pedicels, we first compared the expression pattern of *BRD3* in pedicels and spikelets of NCL1 and CL1. Notably, *BRD3* was up-regulated in pedicels, but not spikelets, of CL1 (Fig. 3F). To confirm this result, we also measured BR content in these tissues of both lines. Consistent with the expression pattern of *BRD3*, the castasterone level was only ~20% lower in CL1 spikelets, yet ~70% lower in CL1 pedicels, compared to NCL1 spikelets and pedicels (Fig. 3G).

We further conducted RNA in situ hybridization to determine the spatiotemporal expression pattern of *BRD3* during panicle development. During the development of NCL1 inflorescences, *BRD3* expression was very weak and not specific to any tissues (Fig. 3, H and I). By contrast, we detected specific signal with

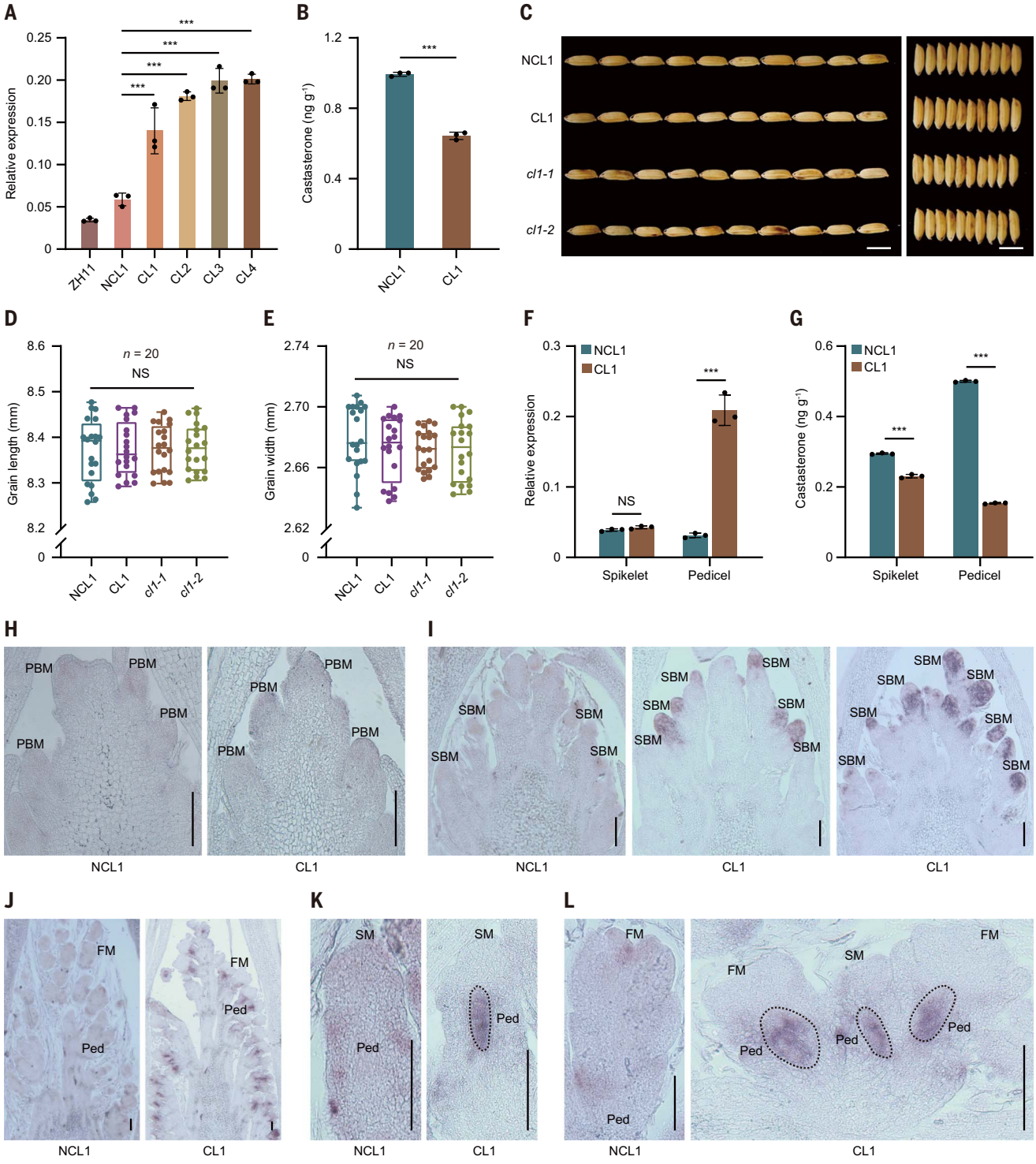

Fig. 3. Specific enhancement of *BRD3* expression in secondary branch meristems and pedicels of CL1. (**A**) Relative expression of *BRD3* in different plants. Error bars indicate SD from three replicate analyses. ***$P < 0.001$ by two-tailed *t* test. (**B**) Quantification of castasterone content in 3- to 5-cm young panicles. Error bars indicate SD from three replicate analyses. ***$P < 0.001$ by two-tailed *t* test. (**C**) Comparison of grain length and width in different plants. Scale bars: 5 mm. (**D** and **E**) Statistical data of grain length (D) and grain width (E) of different plants. NS, not significant. (**F**) Expression of *BRD3* in spikelets and pedicels of NCL1 and CL1. Error bars indicate SD from three replicate analyses. ***$P < 0.001$ by two-tailed *t* test. NS, not significant. (**G**) Quantification of castasterone content in spikelets and pedicels of NCL1 and CL1. Error bars indicate SD from three replicate measurements. ***$P < 0.001$ by two-tailed *t* test. (**H** to **L**) RNA in situ hybridization detecting *BRD3* expression during inflorescence development in NCL1 and CL1. Ped, pedicel. The expression in the presumed pedicel positions is circled. Scale bars: 100 μm.

top-down development in SBM, but not PBM, of CL1 panicles (Fig. 3, H and I). At the stage of SM or FM development, *BRD3* expression was specifically detected at the base of spikelets, corresponding to the pedicel positions, in CL1 but not NCL1 (Fig. 3, J to L). As a negative control, no signal was detected when *BRD3* was used as the sense probe (fig. S18). The strong relationship between *BRD3* expression pattern and plant phenotype suggests that spatial enhancement of *BRD3* expression gives rise to the enhanced grain number, with no impact on grain size.

Spatial expression of GSK2 produces CL

Because spatial up-regulation of BRD3 in CL1 suppresses BR biosynthesis and BRs function through the BR signaling pathway, spatial suppression of BR signaling could also enable CL development. GSK2 is a central negative regulator of BR signaling (*7*), and we have generated many transgenic plants overexpressing the activated form of GSK2 (aGSK2) with or without the fusion of different tags, including FLAG, green fluorescent protein (GFP), and GFP-Myc (*7*, *32*). Whereas most of these plants (*GFP-aGSK2*, *GFP-Myc-aGSK2*, *aGSK2*) showed typical BR-defective phenotypes such as dwarfism and small grains, the *FLAG-aGSK2* overexpression line exhibited dense and compact panicles due to the clustered growth of multiple spikelets (between two and six, three in most cases; Fig. 4, A and B). Immunoblotting analyses confirmed that the phenotype severity coincided with FLAG-aGSK2 protein levels (Fig. 4, C and D). Notably, in all the three lines analyzed, grain number increased from 20 to 31.2% compared to ZH11 (fig. S19). Upon further analysis, one *FLAG-aGSK2* line possessed 62% more secondary branches as well as more spikelets on the secondary branches, with no differences in primary branch numbers, compared to ZH11 (fig. S19). Clearly, many of these characteristics bear a strong resemblance to CL phenotypes.

The BR-related analyses, including lamina inclination assays (fig. S20), evaluation of BR biosynthesis genes (fig. S21), and BR quantifications (fig. S22), all suggested that the FLAG-aGSK2 protein is functional, but its ability to suppress BR signaling is likely weakened. Notably, no difference was detected in term of the grain size and grain weight, and only a slight reduction of plant height was observed in *FLAG-aGSK2* compared to ZH11 (Fig. 4E and fig. S23). The specific enhancement of grain number in *FLAG-aGSK2* resulted in a 14.7 to 27% increase in grain yield per plant compared to ZH11 (fig. S19). We then evaluated GSK2 protein levels in pedicels and spikelets of *FLAG-aGSK2*. In the two independent lines tested, FLAG-aGSK2 accumulated to high levels in pedicels but much less in spikelets (Fig. 4F). By contrast, GFP-aGSK2 was abundant in spikelets but was barely detected in pedicels (Fig. 4G).

We further performed immunofluorescence analysis to compare the spatial distribution of the two fusion proteins in their corresponding plants during panicle development. Notably, whereas both FLAG-aGSK2 and GFP-aGSK2 were not detected at the PBM (Fig. 4H), a strong fluorescent signal was detected at the SBM of only *FLAG-aGSK2*, but not *GFP-aGSK2* (Fig. 4I). The diffused expression of FLAG-aGSK2 in the whole inflorescence is consistent with the overall compact morphology of the panicles (Fig. 4I). With further development, both the proteins were abundantly expressed in the SM as well as the FM, whereas only FLAG-aGSK2, but not GFP-aGSK2, was evidently expressed in pedicels (Fig. 4, J and K). These analyses suggest that the FLAG tag somehow affected the distribution of the fusion protein. Like the case of *BRD3* in NCL1 and CL1, these molecular characterizations were consistent with the plant phenotypes, demonstrating that the CL phenotype is regulated by spatially restricted BR function conferred by specific expression of *BRD3* or FLAG-aGSK2.

Manipulation of BRs modulates CL severity

To assess the impact of BRs on the CL phenotype, we crossed CL1 with two BR-enhanced plants, including *m107*, a mutant carrying overexpressed BR biosynthesis gene *DWARF11* (*D11*) (*33*), and *Gi-2*, an RNA interference (RNAi) line targeting GSK3-like family genes (*7*). Introducing either *m107* or *Gi-2* into CL1 resulted in the elimination of the CL phenotype (fig. S24). In addition, treating CL1 with BL mitigated the CL severity (fig. S25). Moreover, we directly edited *D11* in CL1 using CRISPR-Cas9 and found that knockout of *D11* (CL1 *d11-cc*) substantially intensified the CL phenotype (fig. S26). Notably, a mild *d11* allele displayed a WCL phenotype, and the double mutant *FLAG-aGSK2 d11* exhibited clustered growth of almost all spikelets (fig. S27). Both *FLAG-aGSK2 d11* and CL1 *d11-cc* had short, dense, and erect panicles, yet showing greatly reduced grain size (figs. S26 and S27).

Furthermore, we introduced *FLAG-aGSK2* into CL1 through transformation. Notably, CL1 *FLAG-aGSK2* exhibited markedly heightened CL severity compared to CL1, with clustered growth of up to eight spikelets (Fig. 4, L and M, and fig. S28). These results demonstrated that defective BR signaling amplifies the CL phenotype induced by BR deficiency.

GSK2 phosphorylates OsMADS1 to promote its stability

GSK2 acts as a regulator of various BR responses by targeting multiple downstream components. To delve deeper into the mechanism of BR regulation in CL, we carried out yeast two-hybrid screens using GSK2 as the bait, resulting in the identification of OsMADS1, a potential CL regulator (*34*), as a candidate interacting protein of GSK2. The interaction in yeast was first confirmed using the full-length coding sequence of *OsMADS1* (Fig. 5A). OsMADS1 contains four domains, including the MADS domain (M), the intervening domain (I), the keratin-like domain (K), and the C-terminal domain (C). We generated domain-based deletions and found, only with the presence of M, I, and K domains, that OsMADS1 can interact with GSK2 (Fig. 5B). The interaction was further confirmed in *Nicotiana benthamiana* cells using split-luciferase complementation analysis (fig. S29) and was also verified by pull-down assay, showing that GSK2 fused with glutathione S-transferase (GST-GSK2) was able to interact with OsMADS1 fused with maltose binding protein (MBP-OsMADS1), as well as with MBP-tagged BRASSINAZOLE RESISTANT 1 (MBP-OsBZR1), the well-known GSK2 substrate, as a positive control (Fig. 5C). Together, these analyses demonstrated that GSK2 interacts with OsMADS1.

Previous work has shown that GSK2 kinase could phosphorylate its substrates (*7*). To test whether GSK2 phosphorylates OsMADS1, we conducted in vitro phosphorylation assay using the recombinant proteins GST-GSK2 and MBP-OsMADS1. With the addition of adenosine 5´-triphosphate (ATP), we detected a clear band shift corresponding to the high–molecular-weight bands of OsMADS1, and calf intestinal alkaline phosphatase (CIP) treatment eliminated these bands (fig. S29), demonstrating that GSK2 phosphorylation causes the OsMADS1 mobility shift.

Mass spectrometry analysis of the phosphorylated OsMADS1 identified three phosphorylation sites, located at position 16 for serine (S16), 20 for threonine (T20), and S138 (Fig. 5D and fig. S30). To analyze the effect of these three loci on OsMADS1, we created its phosphor-dead form by mutating all three loci to alanine ($OsMADS1^{TA}$), which cannot be phosphorylated by GSK2 in vitro (fig. S29), and its phosphor-mimic form by mutating to aspartate ($OsMADS1^{TD}$). Mutations of the single site at S138 were also performed, resulting in $OsMADS1^{S138A}$ and $OsMADS1^{S138D}$, respectively. When each of these different forms of OsMADS1 was fused with a GFP tag and introduced into *N. benthamiana*, we found that the fluorescence intensity representing the $OsMADS1^{TD}$ protein level was extraordinarily strong (Fig. 5E). We further detected the expression levels of the different proteins using immunoblotting and obtained the same result, namely, that $OsMADS1^{TD}$ accumulated markedly relative to the wild-type OsMADS1 (Fig. 5F). In addition, both $OsMADS1^{TA}$ and $OsMADS1^{S138A}$ were reduced, whereas $OsMADS1^{S138D}$ tended to be enhanced (Fig. 5F). Moreover, BL treatment markedly induced the instability of the

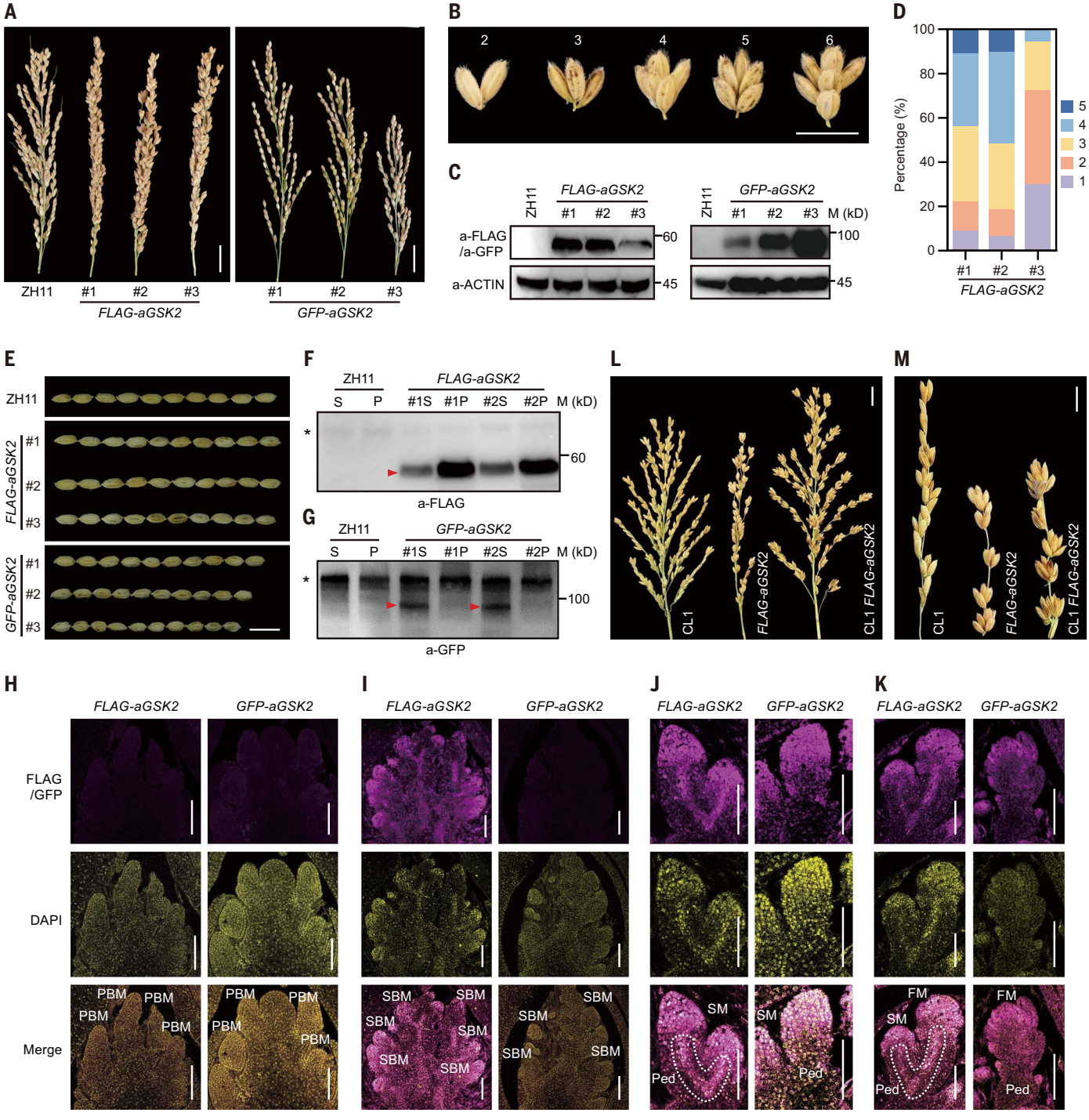

Fig. 4. Spatially specific expression of GSK2 produces CL. (**A**) Panicles of ZH11 and the transgenic plants. Scale bars: 2 cm. (**B**) Different cluster types in *FLAG-aGSK2* plants. Scale bar: 1 cm. (**C**) Detection of the fusion proteins in the transgenic plants by immunoblotting analyses. ACTIN was detected as control. M (kD), marker size indicated in kilodaltons. (**D**) Percentages of grain numbers belonging to different cluster types in the three *FLAG-aGSK2* lines, with 15 panicles analyzed for each line. (**E**) Comparison of grain size in different GSK2-related plants. Scale bar: 5 mm. (**F** and **G**) Detection of the fusion proteins in spikelets (S) and pedicels (P) of the plants by immunoblotting. Asterisk (*) represents a nonspecific band indicating equal protein loading. Arrowheads indicate target protein signals. (**H** to **K**) Immunofluorescence analysis of the fusion proteins during inflorescence development in *FLAG-aGSK2* and *GFP-aGSK2*. Ped, pedicel. The expression in the presumed pedicel positions were circled. Scale bars: 100 μm. (**L** and **M**) Comparison of the panicles and primary branches of CL1, *FLAG-aGSK2*, and the double mutant. Scale bars: 2 cm (L) and 1 cm (M).

OsMADS1-FLAG fusion protein (fig. S29). These results strongly suggested that phosphorylation of OsMADS1 by GSK2 enhances the stability of the OsMADS1 protein.

OsMADS1 accumulates in pedicels of CLs

Given that GSK2 targets and promotes OsMADS1, the OsMADS1 protein should also specifically accumulate in CL plants in the same way that FLAG-aGSK2 protein or BRD3 transcripts do. To test this notion, we analyzed OsMADS1 protein levels in spikelets and pedicels of *FLAG-aGSK2* and *GFP-aGSK2* lines. Compared to wild

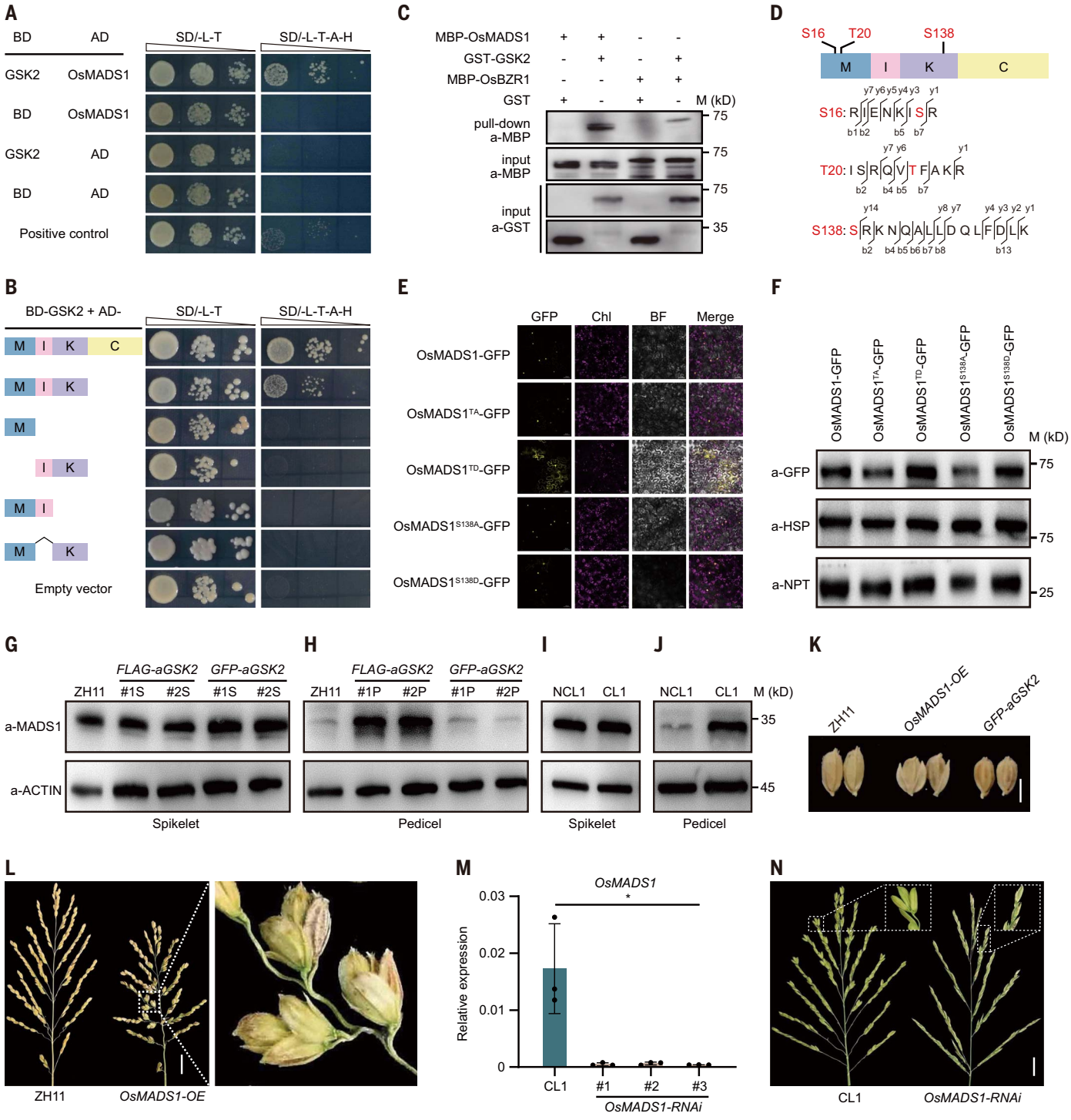

Fig. 5. GSK2 phosphorylates OsMADS1 to mediate CL occurrence. (**A**) Yeast two-hybrid assay showing GSK2-OsMADS1 interaction. SD/-L-T-A-H, synthetic dropout media lacking leucine, threonine, adenine, and histidine. (**B**) Domain-deletion–based yeast two-hybrid assay. (**C**) GST pull-down assay showing GSK2-OsMADS1 interaction. (**D**) Phosphorylation sites and phosphopeptides identified by mass spectrometry analysis. (**E**) Fluorescence intensity analysis of different OsMADS1 forms fused with GFP. OsMADS1^{TA} carries triple alanine at the three phosphorylation sites and OsMADS1^{TD} carries triple aspartate. Chl, chloroplast auto fluorescence; BF, bright field. (**F**) Immunoblotting analysis of the different OsMADS1 forms. HSP (heat shock protein) was detected as the loading control, and NPT (neomycin phosphotransferase) carried by the expression cassette was detected as the internal control. (**G** to **J**) Immunoblotting analyses of OsMADS1 in spikelets (S) and pedicels (P) in different plants. ACTIN was detected to indicate equal loading. (**K**) Grain morphology of ZH11, *OsMADS1-OE*, and a *GFP-aGSK2* line. Scale bar: 0.5 cm. (**L**) CL phenotype of *OsMADS1-OE*. Scale bar: 2 cm. (**M**) Expression analysis of *OsMADS1* in three knockdown lines. Error bars indicate SD from three replicate analyses. *P < 0.05 by two-tailed t test. (**N**) Knockdown of *OsMADS1* abolishes CL phenotype in CL1. Scale bar: 2 cm.

type, in spikelets, OsMADS1 was more abundant in *GFP-aGSK2*, but of similar abundance in *FLAG-aGSK2* (Fig. 5G). By contrast, in pedicels, OsMADS1 strongly accumulated in *FLAG-aGSK2*, but not in *GFP-aGSK2* (Fig. 5H). These data clearly demonstrated that the distribution patterns of OsMADS1 and GSK2 are highly similar in either *GFP-aGSK2* or *FLAG-aGSK2* (Figs. 4, F and G, and 5, G and H). In addition, the distribution patterns are also consistent with the plant phenotypes: *GFP-aGSK2* has smaller grains, whereas *FLAG-aGSK2* has shortened pedicels and normal grain size (Fig. 4E).

We then extended the analysis to CL1 and NCL1. Consistently, OsMADS1 levels were higher in pedicels, but not spikelets, of CL1 compared to NCL1 (Fig. 5, I and J). These patterns were similar to those observed in *FLAG-aGSK2*. Taken together, these results demonstrated that OsMADS1 acts downstream of GSK2 to mediate BR regulation of CL development.

Knockdown of OsMADS1 *abolishes CL phenotype*

Similar to GSK2, OsMADS1 has been characterized as a negative regulator of grain size (*35*, *36*). Furthermore, OsMADS1 has been implicated in regulating meristem identity and potentially enhancing spikelet number (*37*–*39*). Examination of *OsMADS1*-overexpressing plants (*OsMADS1-OE*) confirmed that its grains were notably smaller, like *GFP-aGSK2*, than the wild type ZH11 (Fig. 5K). Notably, the clustered growth of two or three spikelets was clearly observed on almost every panicle, and some branches showed strong resemblance of typical CL characteristics (Fig. 5L). The occurrence of CL phenotype in *OsMADS1-OE* indicated that OsMADS1 mediates GSK2-regulation of the CL trait.

To test that notion, we performed RNAi on *OsMADS1* in CL1 (*OsMADS1-RNAi*). Among the lines generated with suppressed expression of *OsMADS1* (Fig. 5M), the CL phenotype was eliminated (Fig. 5N), indicating that OsMADS1 is necessary for the CL phenotype. These findings, coupled with the analyses, collectively established that OsMADS1 functions downstream of GSK2 to mediate CL development.

Specific accumulation of OsMADS1 *in CL1's SBMs*

To provide direct evidence for the spatial distribution pattern of OsMADS1 protein, we performed immunofluorescence analysis to track the protein abundance during panicle development. Although we could not detect OsMADS1 proteins at the PBM of both CL1 and NCL1, the specific fluorescent signal was detected at the SBM of only CL1, but not NCL1 (Fig. 6, A and B). In addition, the signal was restricted to the apically located SBM, which might be in the transition stage to SM, implying the involvement of OsMADS1 in this process. With further development, OsMADS1 started to be abundantly expressed in the SM as well as the FM in both NCL1 and CL1 (Fig. 6, C and D), consistent with the core function of OsMADS1 as a flower organ regulator reported previously (*37*, *40*–*42*). Notably, a distinct OsMADS1 fluorescent signal was also detected in the center of pedicels of CL1, where the signal was absent in NCL1. This specific expression pattern was fully consistent with the above immunoblotting results and reminiscent of the RNA in situ expression of *BRD3*: Compared to NCL1, both *BRD3* transcripts and OsMADS1 proteins accumulated specifically in the SBM as well as in pedicel-corresponding cells of CL1. Taken together, these results demonstrated that the specific accumulation of OsMADS1 mediates the occurrence of CL caused by the specific distribution of either *BRD3* or GSK2.

OsMADS1 targets a TERMINAL FLOWER1*-like gene*

To gain deeper insights into the function of OsMADS1, a transcriptional factor, we conducted a combined analysis of chromatin immunoprecipitation sequencing (ChIP-seq) and RNA sequencing (RNA-seq), aiming to identify the target genes regulated by OsMADS1. Using young panicles of *OsMADS1-OE* plants (~5 mm in length) as materials, the ChIP-seq analysis detected a total of 1650 OsMADS1-bound peaks associated with 1320 genes (Fig. 6E). Simultaneously, the RNA-seq analysis identified 1354 differentially expressed genes (DEGs) (Fig. 6E). By performing an overlapping analysis of the two datasets, we identified 46 genes as both OsMADS1-bound genes and DEGs regulated by OsMADS1 (Fig. 6E and table S2), which were thus considered as the direct targets of OsMADS1. According to the rice database (https://ricedata.cn/), 15 of them have been functionally characterized (Fig. 6F). Among them, *RICE CENTRORADIALIS2* (*RCN2*) stood out as the most promising target regulating CL development, which ranked third in terms of enrichment fold (~9.84-fold) in the ChIP-seq, and second in terms of expression change (~5.83-fold) in the RNA-seq (Fig. 6F). In addition, further inspection using the Integrated Genome Viewer (*43*) indicated that the binding peak on *RCN2* is highly specific (Fig. 6G). Notably, previous studies have shown that all four *RCN* genes in rice, *RCN1* to *RCN4*, serving as the rice counterparts of *Arabidopsis TERMINAL FLOWER 1* (*TFL1*), play crucial roles in promoting panicle branching by delaying the transition from branch meristem to floral meristem (*25*, *44*, *45*). Overexpression of *RCN2* also leads to a denser panicle morphology, with the number of primary branches comparable to that of wild type, whereas the number of secondary branches and higher-order branches increased substantially, which contributed to an increase in the number of spikelets (*25*, *46*). This observation is compatible with the characteristics of the inflorescence development in the CL plants.

To validate this finding, we performed RNA in situ hybridization to investigate the spatiotemporal expression pattern of *RCN2* during the panicle development of both NCL1 and CL1. In the case of NCL1, *RCN2* expression was not detected in any tissues examined (Fig. 6, H to J), consistent with a previous report (*45*). By contrast, we observed a specific signal in SBM but not in PBM of CL1 panicles (Fig. 6, H and I). We further generated *rcn2-cc* mutants with nucleotide deletions by CRISPR-Cas9 genome editing in CL1 background, and the CL phenotype was eliminated (Fig. 6K and fig. S31). These results indicate that the spatial accumulation of OsMADS1 leads to the specific expression of *RCN2*, resulting in a prolonged transition from SBM to FM and ultimately leading to the production of a greater number of secondary branches and grains.

Harnessing CL *for high-yield breeding*

Our evaluation of NCL1, CL1, *cl1-1*, and *cl1-2* demonstrated the effectiveness of CL in increasing rice yield. Next, we extended our investigation to three popular varieties, including ZH11, 9311, and Yixiang1B (an elite variety widely used as a maintaining line for hybrid breeding). The introduction of the CL trait into these varieties was achieved through backcrossing and selfing until no observable differences other than the panicle morphology remained between the background varieties and their respective introgression lines. Field assessments revealed that introducing CL into any of the three varieties led to significant increases in both grain number and yield per plant (fig. S32).

Gn1a, which corresponds to the defective allele of *CKX2*, has been identified as a key regulator of grain number with high breeding value in rice (*3*). To examine whether CL influences the effect of *Gn1a*, we edited *CKX2* in CL1 using CRISPR–Cas9 (Fig. 7A and fig. S33) and discovered that knockout of *CKX2* still retains the ability to promote grain number in the presence of *CL* (Fig. 7B). The yield per plant further increased by 18.3% compared to CL1 (Fig. 7C). This result inspired us to combine *CL* and *Gn1a* for breeding purposes. Shuhui498 (R498), an NCL elite cultivar with heavy panicles widely cultivated in Southwest China, carries a null allele of *Gn1a*, which confers enhanced grain number and lodging resistance (*47*). By crossing CL1 with R498, we successfully developed a new rice strain named CL5 (Fig. 7D). This strain combined the benefits of *Gn1a* and *CL*, as well as several additional favorable-trait gene alleles derived from either CL1 or R498 (Fig. 7D and fig. S34). In Beijing, CL5 had 106.3 and 48% more grains per panicle than R498 and CL1, respectively. In Sanya, CL5 also showed significant improvement in grain

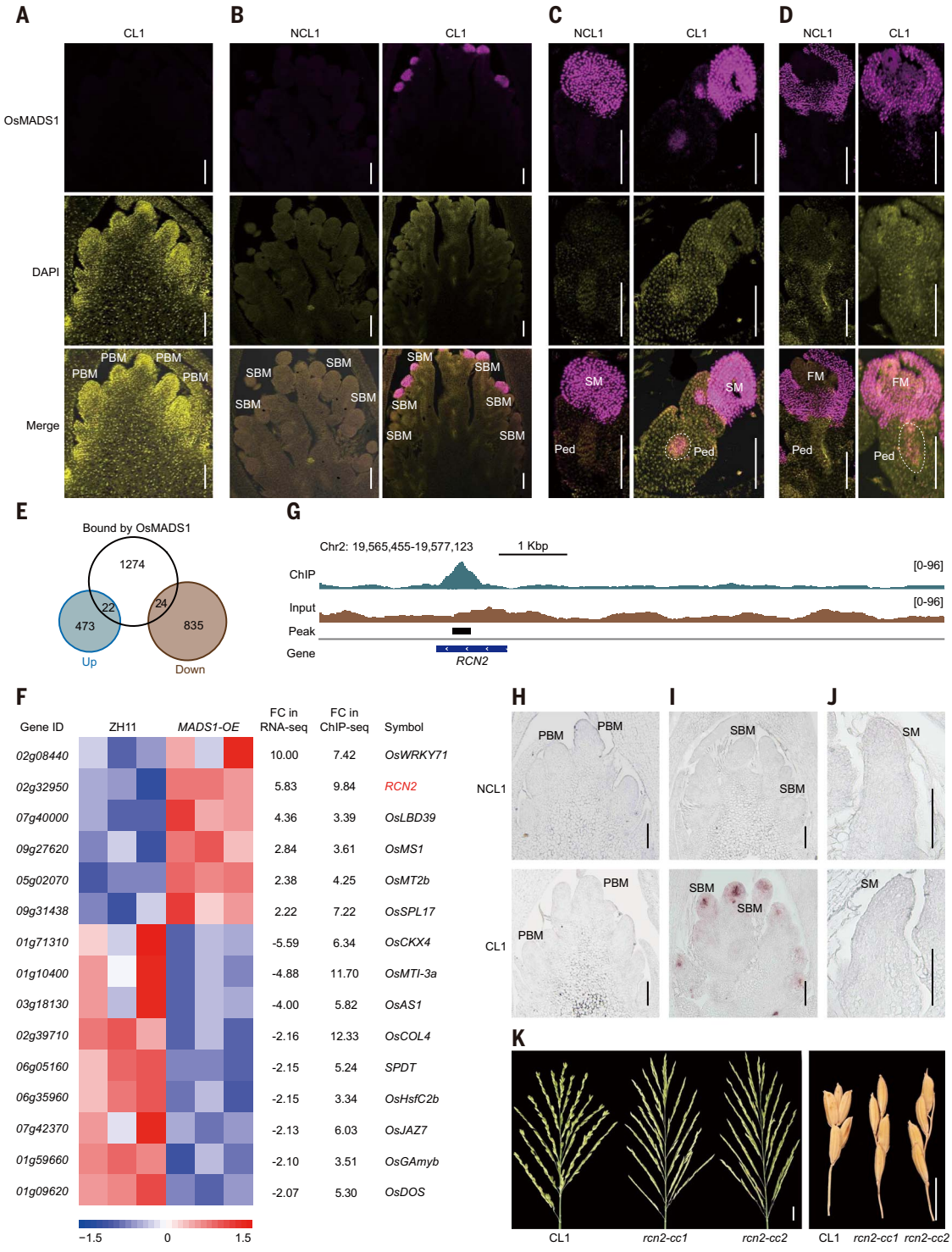

Fig. 6. OsMADS1 targets and up-regulates *RCN2*. (**A** to **D**) Immunofluorescence analysis of OsMADS1 proteins during inflorescence development in NCL1 and CL1. Ped, pedicel. The expression of OsMADS1 in the presumed pedicel positions is circled. Scale bars: 100 μm. (**E**) Venn diagram showing the overlap between OsMADS1-bound genes identified by ChIP-seq and DEGs in *OsMADS1-OE* young panicles relative to ZH11 as identified by RNA-seq. (**F**) Heatmap of the 15 functionally characterized genes both as OsMADS1-bound genes and OsMADS1-regulated DEGs. Values indicating fold change (FC) in RNA-seq and ChIP-seq are shown. *RCN2* is highlighted. (**G**) Visualization of OsMADS1-bound peak on *RCN2* in Integrative Genomics Viewer. The genomic region for inspection is indicated, and sequencing of the input DNA was included as a control. Numbers (0-96) indicate the range on the vertical axis for comparing the signal strength. (**H** to **J**) RNA in situ hybridization detecting *RCN2* expression during inflorescence development in NCL1 and CL1. Scale bars: 100 μm. (**K**) Panicle morphology of *rcn2-cc* lines generated by CRISPR-Cas9, with secondary branches at harvesting stage shown on right. Scale bars: 2 cm (left) and 1 cm (right).

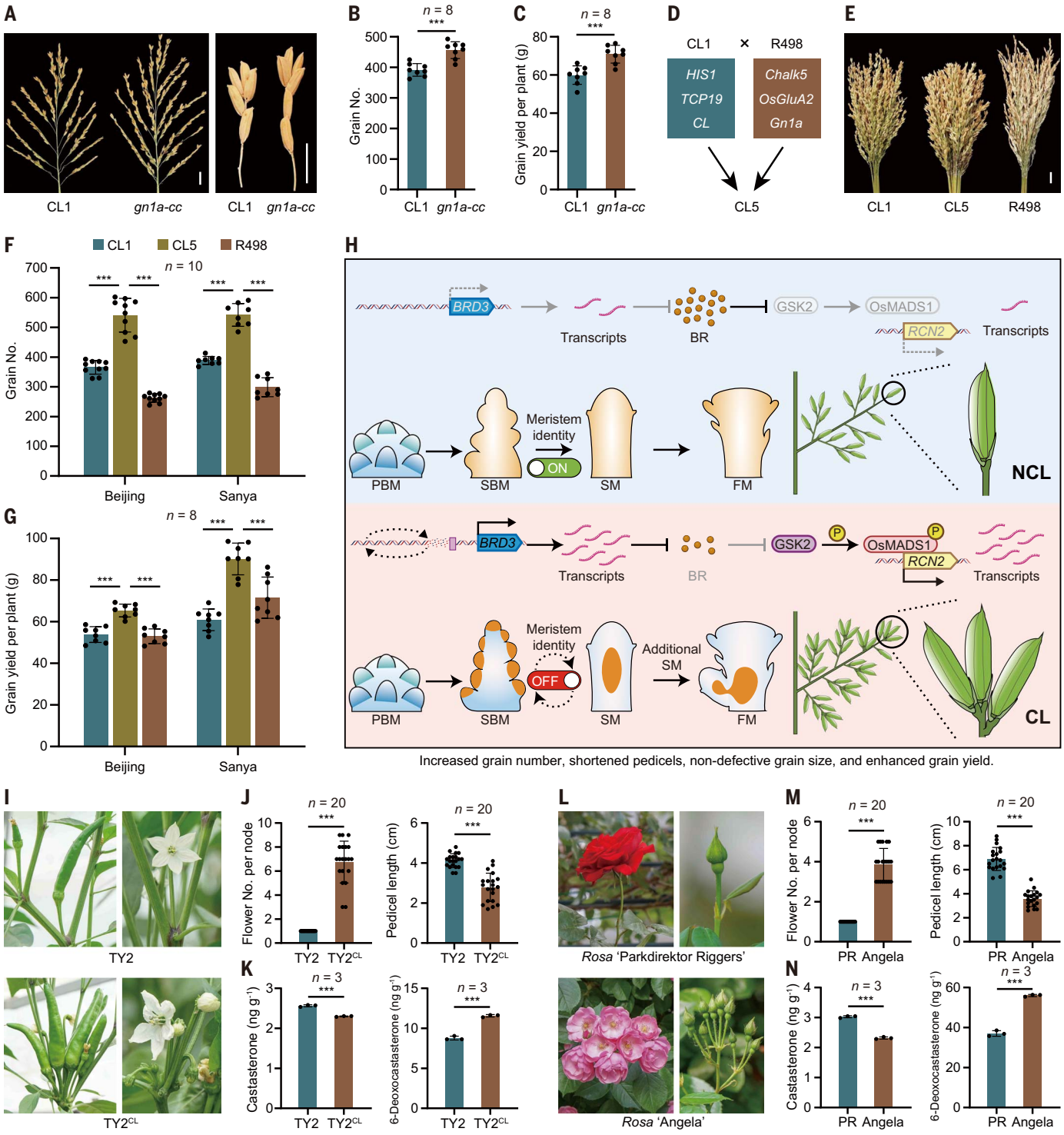

Fig. 7. Utilizing CL for high-yield breeding. (**A**) Panicle morphology of *gnla*-cc under CL1, with secondary branches shown. Scale bars: 2 cm (left) and 1 cm (right). (**B** and **C**) Grain number per panicle (B) and grain yield per plant (C) of CL1 and *gn1a-cc*. (**D**) Source of several beneficial gene alleles in CL5. (**E**) Comparison of a collection of 10 panicles. Scale bar: 2 cm. (**F** and **G**) Grain number per panicle (F) and grain yield per plant (G) of CL1, CL5, and R498. (**H**) Schematic diagram illustrating the major findings of this study. Large structural variations in CL specifically activate *BRD3* in certain tissues (orange), prolonging the transition from SBMs to SMs through a series of molecular events, resulting in increased SBMs and additional SMs. (**I**) Comparison of common pepper Tianyu 2 (TY2) and cluster pepper TY2^{CL}. (**J**) Flower number from one node and pedicel length between TY2 and TY2^{CL}. (**K**) BR quantification in pedicels. (**L**) Comparison of *Rosa* "Parkdirektor Riggers" (PR) and *Rosa* "Angela". (**M**) Flower number from one node and pedicel length between PR and Angela. (**N**) BR quantification in pedicels. For column charts, ***P < 0.001 generated by two-tailed t test.

number with 81.5 and 39.7% more grains per panicle compared to R498 and CL1, respectively (Fig. 7, E and F). In addition, CL5 possessed other advantageous traits such as a thick culm, heavier grains (fig. S35), and high yield (Fig. 7G), illustrating the promising potential of combining *CL* and *Gn1a* for enhancing rice yield.

BR alteration in clustered growth in other species

Although we demonstrated that BR depletion controls CL in rice (Fig. 7H), we wanted to know whether this represent a general mechanism underlying clustered growth across plant species. Cluster peppers (*Capsicum annuum* L. var. *fasciculatum*) display multiple flowers clustered on a single flower bud formation node, whereas common peppers (*Capsicum annuum* L.) have only one flower attached to the node. We measured the BR content in pedicels of Tianyu 2 (TY2), a common pepper, and $TY2^{CL}$, a cluster pepper showing clustered flowers and shortened pedicels while closely resembling TY2 in vegetative and reproductive morphology (Fig. 7, I and J). Like CL1 and NCL1, the castasterone level was lower in $TY2^{CL}$ pedicels compared to TY2 (Fig. 7K). Conversely, the 6-deoxocastasterone level, the precursor of castasterone, was higher in $TY2^{CL}$ pedicels (Fig. 7K), indicating a possible loss of function in the BR synthase responsible for converting 6-deoxocastasterone to castasterone.

We also measured the BR content in the pedicels of the vine *Rosa chinensis* (*Rosa* "Parkdirektor Riggers") and the vine *Rosa* sp. (*Rosa* "Angela"), which displays the clustered flowers and shortened pedicels (Fig. 7, L and M). Like TY2 and $TY2^{CL}$, the castasterone level in *Rosa* "Angela" pedicels was lower compared to *Rosa* "Parkdirektor Riggers," whereas the 6-deoxocastasterone level exhibited the opposite trend (Fig. 7N). These consistent findings indicate that BR distribution may play a general role in regulating the clustered growth and inflorescence structure.

Discussion

We unraveled the genetic basis underlying the historic CL germplasm, shedding light on the development of CL and its association with enhanced grain number, a crucial determinant of yield. We demonstrated that defective BR catabolism or signaling contributes to spikelet clustering and increased grain number, mediated by the specific spatial expression of *BRD3* transcripts, GSK2 protein, OsMADS1 protein, and *RCN2* transcripts. During CL's panicle development, the activation of *BRD3* in SBM triggers BR degradation, which enhances GSK2 stability, promotes OsMADS1 accumulation, and subsequently increases *RCN2* expression. As a result, the identity of SM is suppressed, leading to a delayed transition from BM to SM, ultimately yielding more SBMs and additional SMs formed adjacent to the terminal spikelet (Fig. 7H). Overall, our study exemplifies the successful utilization of natural rice germplasm resources harboring beneficial alleles to breed superior rice strains, from gene cloning to the dissection of the underlying molecular mechanisms.

KNOX transcription factors play a crucial role in the establishment and maintenance of the shoot apical meristem (SAM) (*48*). In *Arabidopsis*, BREVIPEDICELLUS (BP), a KNOX transcription factor, has been shown to regulate pedicel development (*48*). In rice, ORYZA SATIVA HOMEBOX1 (OSH1), the closest ortholog of BP, targets and activates BR catabolic genes, including *BRD3*, to maintain SAM activity (*49*). Therefore, the degradation of BRs should also promote the activity of SBM and SM. In our study, we observed an increase in grain number accompanied by shortened pedicels, and the expression of *BRD3* was detected sequentially in both the meristem cells and pedicel cells, suggesting a potential derivation of pedicels from meristem cells. Our findings imply that large structural variations preceding the *BRD3* gene may be responsible for the spatially specific increase in *BRD3* expression observed in CL. Although the detailed mechanism requires further exploration, one possibility is that these structural variations enhance chromatin accessibility, allowing the entry of transcription factors, such as OSH1, to promote *BRD3* expression.

Constitutive activation of *BRD3* in a transferred DNA (T-DNA) insertion mutant results in severe developmental defects, whereas moderately increased expression of *BRD3* in the heterozygote leads to higher grain number but smaller grains (*29*). Therefore, the practical application of *CL* in crop improvement can be attributed to two main factors related to *BRD3* expression: spatially specific expression and optimal expression. The resulting spatial distribution of BRs provides beneficial effects while preventing the reduction in grain size typically observed in BR-defective mutants, showcasing its practical applicability in crop improvement. Together with our previous research on the distribution of cytokinins and auxins (*50*, *51*), this work highlights the potential of optimizing hormone distributions to achieve desirable traits while mitigating negative associations in crop improvement efforts. Improving grain yield is intricately linked to expanding source supply, influenced by various factors such as source capacity, growth conditions (light, water, temperature, nutrients), and fertilizers. Although introduction of CL into several different modern cultivars all resulted in yield improvement, we observed distinct effects in different locations and genetic backgrounds. Considering that CL is influenced by BR content and each rice may exhibit variable BR levels, it is crucial to extensively test the effectiveness of CL in diverse contexts.

Materials and methods summary

Plant growth, suppressor screening, and segregating populations

For field plot analysis, each material was planted with a row interspace of 20 cm and plant interspace of 17.1 cm, with ~33 plants per square meter. At least four plots were planted as biological replicates. The border plants were removed from each plot to avoid margin effects during measurements. For experiments requiring seedling analysis, plants were grown in a growth chamber at 30°C with 10 hours light for day and 28°C with 14 hours dark for night. Half-strength Murashige and Skoog (½-MS) solution was provided as the nutrient source. For suppressor screening, dry CL1 seeds were incubated in sodium azide (1 mM in phosphate buffer pH 3.0) for 6 hours. After a thorough wash with tap water, the seeds were germinated and planted. A total of 10,000 individual lines were harvested, and 16 plants of each line were grown for mutant screening. Four segregating populations were generated by crossing CL1 with ZH11, 9311, *cl1-1*, and *cl1-2*, respectively. For each population, pooled DNAs from NCL plants and CL plants were prepared for BSA. Numbers of individual plants used for DNA pools from each population were as follows: 36 NCL and 34 CL from CL1 × ZH11, 24 NCL and 31 CL from CL1 × 9311, 31 NCL and 33 CL from CL1 × *cl1-1*, and 20 NCL and 19 CL from CL1 × *cl1-2*.

RNA in situ hybridization

Specific fragments of *BRD3* and *RCN2* were amplified by PCR with primers listed in table S1. The fragments were subsequently inserted into the pEASY-Blunt Simple Cloning Vector (TransGen) for in vitro RNA transcription. Sense and antisense RNA probes were produced using T7 transcriptase and labeled with digoxigenin (Roche). Young panicle tissues from NCL1 and CL1 were collected and fixed in FAA (45% ethanol, 6% glacial acetic acid, and 5% formaldehyde) at 4°C overnight in a vacuum, dehydrated, and embedded in Paraplast Plus (Sigma-Aldrich, St. Louis). Tissue sections were prepared using a microtome (RM2235; Leica, Wetzlar) and then affixed to Poly-Prep slides (Sigma-Aldrich, St. Louis).

In vitro phosphorylation and mass spectrum analysis

One microgram of GST-GSK2 and 2 μg of MBP-OsMADS1 or $MBP\text{-}OsMADS1^{TA}$ were incubated in the kinase buffer [10 mM Tris-HCl (pH 7.4), 50 mM NaCl, 6 mM $MgCl_2$, 0.5 mM dithiothreitol] with or without ATP and CIP (NEB) at 30°C for 2 hours. Phos-tag™ SDS–polyacrylamide gel electrophoresis (PAGE) was used to separate the phosphorylation protein following the instruction of the product Phos-tag™ Acrylamide (Wako). To identify the phosphorylation sites, 4 μg of recombinant

MBP-OsMADS1 or MBP-OsMADS1^{TA} proteins were phosphorylated by 2 μg of GST-GSK2 for 1 hour in vitro. Phos-tag^{TM} SDS-PAGE was used to separate the phosphorylation protein. The target protein bands were cut after one-step blue staining (Biotium). The LC-MS/MS detection and analysis were conducted by the Shanghai Luming Biological Technology Co., Ltd. (Shanghai, China).

Immunofluorescence detection

An 8-μm-thick section was cut from paraffin-embedded young panicle tissues for detection. The slides were deparaffinized, rehydrated, and subjected to epitope retrieval by boiling in 1× All-purpose Powerful Antigen Retrieval Solution (Beyotime) for 20 min at 95°C, and set to cool for 30 to 40 min. The slides were washed two times in 1× Immunol Staining Wash Buffer (Beyotime) for 10 min each, blocked in Immunol Staining Blocking Buffer (Beyotime) for 60 min at room temperature, and then rinsed two times in 1× Immunol Staining Wash Buffer (Beyotime) for 10 min each. The primary antibody for OsMADS1 (1:50; Abclonal, Cat#A20328), or for FLAG-aGSK2 (anti-FLAG, 1:50; Sigma, Cat#F1804), or for GFP-aGSK2 (anti-GFP, 1:50; Abmart, Cat#M2004l), was used for incubation overnight at 4°C. The specimen was rinsed three times in 1× Immunol Staining Wash Buffer (Beyotime) for 5 min each, and then incubated in the Goat anti-Rabbit IgG (H+L) Highly Cross-Adsorbed Secondary Antibody, Alexa Fluor^{TM} Plus 555 (1:400; Invitrogen, Cat#A32732) or Goat anti-Mouse IgG (H+L) Highly Cross-Adsorbed Secondary Antibody, Alexa Fluor Plus 488 (1:400; Invitrogen, Cat#A32723) at room temperature for 60 min in dark. The slides were further rinsed three times in 1× Immunol Staining Wash Buffer (Beyotime) for 5 min each, and then covered using coverslips filled with Antifade Mounting Medium with 4′,6-diamidino-2-phenylindole (DAPI; Beyotime). Fluorescence was captured with a confocal laser scanning microscope (LSM 980; Zeiss, Oberkochen).

ChIP-seq and RNA-seq

About 1 g of young panicles at the 5-mm stage of *OsMADS1-OE* were used for ChIP-seq. Tissue fixation, nuclei extraction, and chromatin immunoprecipitation were performed using anti-OsMADS1 (1:100; Abclonal, Cat#A20328) antibody. The ChIP-seq DNA libraries were sequenced using the Illumina HiSeqTM2000 platform. After quality control, BWA software was used to align the clean reads against the Nipponbare reference genome (IRGSP1.0). MACS software was used for peak calling on a genome-wide basis, and the threshold for screening significant peak was q-value < 0.05. Significant peaks were assigned to the nearest gene. For RNA-seq, about 1 g of young panicles at the 5-mm stage of *OsMADS1-OE* and ZH11 were collected, and total RNA was extracted from each of three biological replicates using TRIzol reagent (Invitrogen). Sequencing libraries were generated using NEBNext Ultra RNA Library Prep Kit for Illumina (NEB), following the manufacturer's recommendations, and sequenced on Illumina NovaSeq platform. After cleaning up raw sequence reads, the clean reads were mapped to the Nipponbare reference genome (IRGSP1.0). The differentially expressed genes were analyzed using the edgeR package. Genes with a false discovery rate (FDR) < 0.05 and $\log_2$(fold change) > 1 were assigned as differentially expressed.

REFERENCES AND NOTES

1. T. Sasaki, B. Burr, International Rice Genome Sequencing Project: The effort to completely sequence the rice genome. *Curr. Opin. Plant Biol.* **3**, 138–142 (2000). doi: 10.1016/S1369-5266(99)00047-3; pmid: 10712951
2. X. Huang *et al*., Natural variation at the *DEP1* locus enhances grain yield in rice. *Nat. Genet.* **41**, 494–497 (2009). doi: 10.1038/ng.352; pmid: 19305410
3. M. Ashikari *et al*., Cytokinin oxidase regulates rice grain production. *Science* **309**, 741–745 (2005). doi: 10.1126/science.1113373; pmid: 15976269
4. E. J. Kim, E. Russinova, Brassinosteroid signalling. *Curr. Biol.* **30**, R294–R298 (2020). doi: 10.1016/j.cub.2020.02.011; pmid: 32259497
5. H. Tong, C. Chu, Functional specificities of brassinosteroid and potential utilization for crop improvement. *Trends Plant Sci.* **23**, 1016–1028 (2018). doi: 10.1016/j.tplants.2018.08.007; pmid: 30220494
6. T. M. Nolan, N. Vukašinović, D. Liu, E. Russinova, Y. Yin, Brassinosteroids: Multidimensional regulators of plant growth, development, and stress responses. *Plant Cell* **32**, 295–318 (2020). doi: 10.1105/tpc.19.00335; pmid: 31776234
7. H. Tong *et al*., DWARF AND LOW-TILLERING acts as a direct downstream target of a GSK3/SHAGGY-like kinase to mediate brassinosteroid responses in rice. *Plant Cell* **24**, 2562–2577 (2012). doi: 10.1105/tpc.112.097394; pmid: 22685166
8. J. Li, K. H. Nam, Regulation of brassinosteroid signaling by a GSK3/SHAGGY-like kinase. *Science* **295**, 1299–1301 (2002). doi: 10.1126/science.1065769; pmid: 11847343
9. J. H. Youn, T. W. Kim, Functional insights of plant GSK3-like kinases: Multi-taskers in diverse cellular signal transduction pathways. *Mol. Plant* **8**, 552–565 (2015). doi: 10.1016/j.molp.2014.12.006; pmid: 25655825
10. Z. Hong *et al*., A rice brassinosteroid-deficient mutant, *ebisu dwarf* (*d2*), is caused by a loss of function of a new member of cytochrome P450. *Plant Cell* **15**, 2900–2910 (2003). doi: 10.1105/tpc.014712; pmid: 14615594
11. S. Tanabe *et al*., A novel cytochrome P450 is implicated in brassinosteroid biosynthesis via the characterization of a rice dwarf mutant, *dwarf11*, with reduced seed length. *Plant Cell* **17**, 776–790 (2005). doi: 10.1105/tpc.104.024950; pmid: 15705958
12. C. Yamamuro *et al*., Loss of function of a rice *brassinosteroid insensitive1* homolog prevents internode elongation and bending of the lamina joint. *Plant Cell* **12**, 1591–1606 (2000). doi: 10.1105/tpc.12.9.1591; pmid: 11006334
13. L. Song *et al*., Reducing brassinosteroid signalling enhances grain yield in semi-dwarf wheat. *Nature* **617**, 118–124 (2023). doi: 10.1038/s41586-023-06023-6; pmid: 37100915
14. J. Tian *et al*., Teosinte ligule allele narrows plant architecture and enhances high-density maize yields. *Science* **365**, 658–664 (2019). doi: 10.1126/science.aax5482; pmid: 31416957
15. T. Sakamoto *et al*., Erect leaves caused by brassinosteroid deficiency increase biomass production and grain yield in rice. *Nat. Biotechnol.* **24**, 105–109 (2006). doi: 10.1038/nbt1173; pmid: 16369540
16. K. Ramiah, S. Jobitharaj, S. D. Mudaliar, Inheritance of characters in rice, Part IV. *Mem. Dept. Agric. India Bot. Ser.* **18**, 229–259 (1931).
17. N. E. Jodon, Inheritance and linkage relationships of a chlorophyll mutation in rice. *Agron. J.* **32**, 342–346 (1940). doi: 10.2134/agronj1940.00021962003200050004x
18. N. E. Jodon, Inheritance of some of the more striking characters in rice. *J. Hered.* **48**, 181–192 (1957). doi: 10.1093/oxfordjournals.jhered.a106718
19. S. Nagao, M. E. Takahashi, Genetical studies on rice plant, XXVII. Trial construction of twelve linkage groups in Japanese rice. *J. Fac. Agric. Hokkaido Univ.* **53**, 72–130 (1963).
20. H. Chen, G. Liu, X. Zhu, S. Min, Observation and genetically analysis on character of clustered spikelets in rice. *J. Nanjing Agric. Univ.* **25**, 116–118 (2002).
21. C. Tian *et al*., Genetic analysis and preliminary gene mapping of rice clustered spikelet mutant. *Mol. Plant Breed.* **8**, 29–34 (2010).
22. Y. Zhang *et al*., Development of NILs with *Cl*-gene of rice restorer and evaluation on the near-isogenic level. *Acta Agron. Sin.* **32**, 397–401 (2006).
23. L. Y. Zheng *et al*., Morphology and mapping analysis of rice (*Oryza sativa* L.) *clustered spikelets* (*Cl*) mutant. *Chin. Sci. Bull.* **48**, 559–562 (2003). doi: 10.1360/03tb9119
24. Y. Zheng *et al*., Fine mapping and candidate gene analysis of clustered spikelet gene *OsCl-6* in rice (*Oryza sativa*). *J. Agric. Biotechnol.* **26**, 1116–1123 (2018).
25. M. Nakagawa, K. Shimamoto, J. Kyozuka, Overexpression of *RCN1* and *RCN2*, rice *TERMINAL FLOWER 1/CENTRORADIALIS* homologs, confers delay of phase transition and altered panicle morphology in rice. *Plant J.* **29**, 743–750 (2002). doi: 10.1046/j.1365-313X.2002.01255.x; pmid: 12148532
26. P. Prusinkiewicz, Y. Erasmus, B. Lane, L. D. Harder, E. Coen, Evolution and development of inflorescence architectures. *Science* **316**, 1452–1456 (2007). doi: 10.1126/science.1140429; pmid: 17525303
27. P. McSteen, D. Laudencia-Chingcuanco, J. Colasanti, A floret by any other name: Control of meristem identity in maize. *Trends Plant Sci.* **5**, 61–66 (2000). doi: 10.1016/S1360-1385(99)01541-1; pmid: 10664615
28. W. Wang *et al*., Genomic variation in 3,010 diverse accessions of Asian cultivated rice. *Nature* **557**, 43–49 (2018). doi: 10.1038/s41586-018-0063-9; pmid: 29695866
29. W. Qian *et al*., Novel rice mutants overexpressing the brassinosteroid catabolic gene *CYP734A4*. *Plant Mol. Biol.* **93**, 197–208 (2017). doi: 10.1007/s11103-016-0558-4; pmid: 27815670
30. T. Sakamoto *et al*., Rice CYP734As function as multisubstrate and multifunctional enzymes in brassinosteroid catabolism. *Plant J.* **67**, 1–12 (2011). doi: 10.1111/j.1365-313X.2011.04567.x; pmid: 21418356
31. H. A. Agrama *et al*., Genetic assessment of a mini-core subset developed from the USDA rice genebank. *Crop Sci.* **49**, 1336–1346 (2009). doi: 10.2135/cropsci2008.06.0551
32. D. Liu *et al*., Diversification of plant agronomic traits by genome editing of brassinosteroid signaling family genes in rice. *Plant Physiol.* **187**, 2563–2576 (2021). doi: 10.1093/plphys/kiab394; pmid: 34618079
33. H. Tong *et al*., Brassinosteroid regulates cell elongation by modulating gibberellin metabolism in rice. *Plant Cell* **26**, 4376–4393 (2014). doi: 10.1105/tpc.114.132092; pmid: 25371548
34. L. Wang *et al*., Ectopic expression of *OsMADS1* caused dwarfism and spikelet alteration in rice. *Plant Growth Regul.* **81**, 433–442 (2017). doi: 10.1007/s10725-016-0220-9
35. Q. Liu *et al*., G-protein βγ subunits determine grain size through interaction with MADS-domain transcription factors in rice. *Nat. Commun.* **9**, 852 (2018). doi: 10.1038/s41467-018-03047-9; pmid: 29487282
36. J. Yu *et al*., Alternative splicing of *OsLG3b* controls grain length and yield in japonica rice. *Plant Biotechnol. J.* **16**, 1667–1678 (2018). doi: 10.1111/pbi.12903; pmid: 29479793
37. J. S. Jeon *et al*., *leafy hull sterile1* is a homeotic mutation in a rice MADS box gene affecting rice flower development. *Plant Cell* **12**, 871–884 (2000). doi: 10.1105/tpc.12.6.871; pmid: 10852934
38. K. Prasad, S. Parameswaran, U. Vijayraghavan, *OsMADS1*, a rice MADS-box factor, controls differentiation of specific cell types in the lemma and palea and is an early-acting regulator of inner floral organs. *Plant J.* **43**, 915–928 (2005). doi: 10.1111/j.1365-313X.2005.02504.x; pmid: 16146529
39. D. Ren, Y. Li, G. He, Q. Qian, Multifloret spikelet improves rice yield. *New Phytol.* **225**, 2301–2306 (2020). doi: 10.1111/nph.16303; pmid: 31677165
40. S. T. Malcomber, E. A. Kellogg, Heterogeneous expression patterns and separate roles of the SEPALLATA gene *LEAFY HULL STERILE1* in grasses. *Plant Cell* **16**, 1692–1706 (2004). doi: 10.1105/tpc.021576; pmid: 15208396
41. K. Prasad, P. Sriram, C. S. Kumar, K. Kushalappa, U. Vijayraghavan, Ectopic expression of rice *OsMADS1* reveals

a role in specifying the lemma and palea, grass floral organs analogous to sepals. *Dev. Genes Evol.* **211**, 281–290 (2001). doi: 10.1007/s004270100153; pmid: 11466523
42. I. Khanday, S. R. Yadav, U. Vijayraghavan, Rice *LHS1/OsMADS1* controls floret meristem specification by coordinated regulation of transcription factors and hormone signaling pathways. *Plant Physiol.* **161**, 1970–1983 (2013). doi: 10.1104/pp.112.212423; pmid: 23449645
43. J. T. Robinson *et al*., Integrative genomics viewer. *Nat. Biotechnol.* **29**, 24–26 (2011). doi: 10.1038/nbt.1754; pmid: 21221095
44. W. Zhu *et al*., Rice *SEPALLATA* genes *OsMADS5* and *OsMADS34* cooperate to limit inflorescence branching by repressing the *TERMINAL FLOWER1*-like gene *RCN4*. *New Phytol.* **233**, 1682–1700 (2022). doi: 10.1111/nph.17855; pmid: 34767634
45. S. Zhang *et al*., *TFL1/CEN*-like genes control intercalary meristem activity and phase transition in rice. *Plant Sci.* **168**, 1393–1408 (2005). doi: 10.1016/j.plantsci.2004.10.022
46. X. Yang *et al*., miR156f integrates panicle architecture through genetic modulation of branch number and pedicel length pathways. *Rice (N. Y.)* **12**, 40 (2019). doi: 10.1186/s12284-019-0299-5; pmid: 31147794
47. B. Tu *et al*., Loss of *Gn1a/OsCKX2* confers heavy-panicle rice with excellent lodging resistance. *J. Integr. Plant Biol.* **64**, 23–38 (2022). doi: 10.1111/jipb.13185; pmid: 34783157
48. S. J. Douglas, C. D. Riggs, Pedicel development in *Arabidopsis thaliana*: Contribution of vascular positioning and the role of the *BREVIPEDICELLUS* and *ERECTA* genes. *Dev. Biol.* **284**, 451–463 (2005). doi: 10.1016/j.ydbio.2005.06.011; pmid: 16038894
49. K. Tsuda, N. Kurata, H. Ohyanagi, S. Hake, Genome-wide study of *KNOX* regulatory network reveals brassinosteroid catabolic genes important for shoot meristem function in rice. *Plant Cell* **26**, 3488–3500 (2014). doi: 10.1105/tpc.114.129122; pmid: 25194027
50. L. Liu *et al*., Activation of *Big Grain1* significantly improves grain size by regulating auxin transport in rice. *Proc. Natl. Acad. Sci. U.S.A.* **112**, 11102–11107 (2015). doi: 10.1073/pnas.1512748112; pmid: 26283354
51. W. Yin *et al*., ARGONAUTE2 enhances grain length and salt tolerance by activating *BIG GRAIN3* to modulate cytokinin distribution in rice. *Plant Cell* **32**, 2292–2306 (2020). doi: 10.1105/tpc.19.00542; pmid: 32409321
52. X. Zhang, Nanopore sequencing, RNA-seq and ChIP-seq data, *Zenodo* (2024); doi: 10.5281/zenodo.10574305
53. X. Zhang, BSA data,*Zenodo* (2024); doi: 10.5281/zenodo.10574366
54. X. Zhang, Resequencing data of CL1, Zenodo (2024); doi: 10.5281/zenodo.10574479

ACKNOWLEDGMENTS

We thank Q. Li (Yangzhou University) for grain quality evaluation, Y. Li (Southwest University) for providing *OsMADS1-OE* lines, C. Sun (Sichuan Agricultural University) for sequence resemblance, G. Jiang (IGDB-CAS) and W. Wang (ICS-CAAS) for providing CL plants, H. Wu (IVF-CAAS) for providing peppers, C. Tian (IVF-CAAS) for suggestion of rose, and B. Cai (Wuhan Greensword Creation Technology Co. Ltd.) for BR quantification. **Funding:** This work was supported by National Natural Science Foundation (U21A20208, 32272141), Hainan Seed Industry Laboratory (B23CJ0208), Innovation Program of Chinese Academy of Agricultural Sciences, and "5511" Collaborative Innovation Project (XTCXGC2021001). **Author contributions:** H.T. conceived and designed the study. X.Z., W.M., and D.L. performed experiments. Y.Y., Z.C., X.M., W.Y., M.N., N.D., and J.L. and Z.L. provided assistance. D.P., W.S., Y.Q.L., and M.Z. conducted field tests and breeding. X.Z., W.M., and H.T. analyzed the data and wrote the manuscript. H.T., Q.Q., M.Z., and C.C. cosupervised the study. **Competing interests:** H.T., X.Z., D.L., W.M., W.Y., M.N., N.D., J.L., and Y.Y. are inventors on a granted patent in China related to this work (no. ZL202210239578.7). The other authors declare that they have no competing interests. **Data and materials availability:** All sequencing data generated in this paper have been deposited and made available at Zenodo (*52*–*54*). All other data are available in the main text or the supplementary materials.

SUPPLEMENTARY MATERIALS

science.org/doi/10.1126/science.adk8838
Materials and Methods
Figs. S1 to S35
Tables S1 and S2
References (*55*–*73*)
MDAR Reproducibility Checklist

Submitted 15 September 2023; accepted 29 January 2024
10.1126/science.adk8838